Additive Manufactured Polyether-ether-ketone Composite Scaffolds with Hydroxyapatite Filler and Porous Structure Promoted the Integration with Soft Tissue

Changning Sun[1,2,5#], Huiyu Zhao[3,#], Lei Wang[4], Jinghua Zhang[1,2], Jibao Zheng[1,2], Zijian Yang[3], Lijun Huang[4], Ling Wang[1,2,*], Chaozong Liu[5], Dichen Li[1,2,*] , Qingchu Li[3,*]

[1] State Key Laboratory for Manufacturing System Engineering, School of Mechanical Engineering, Xi'an Jiaotong University, 710054, Xi'an, ShaanXi, China

[2] National Medical Products Administration (NMPA) Key Laboratory for Research and Evaluation of Additive Manufacturing Medical Devices, Xi'an Jiaotong University, 710054, Xi'an, ShaanXi, China

[3] Academy of Orthopedics, Orthopaedic Hospital of Guangdong Province, The Third Affiliated Hospital of Southern Medical University, 510665, Guangzhou, China

[4] Department of Thoracic Surgery, Tangdu Hospital, Fourth Military Medical University, 710038, Xi'an, China

[5] Institute of Orthopaedic & Musculoskeletal, University College London, Royal National Orthopaedic Hospital, Stanmore HA7 4LP, UK

1   *** Corresponding Author:**

2   **Prof. Ling Wang**

3   Email: menlwang@mail.xjtu.edu.cn

4   State Key Laboratory for Manufacturing System Engineering

5   School of Mechanical Engineering

6   Xi'an Jiaotong University,

7   China

8

9   **Prof. Dichen Li**

10   Email: dcli@mail.xjtu.edu.cn

11   State Key Laboratory for Manufacturing System Engineering

12   School of Mechanical Engineering

13   Xi'an Jiaotong University,

14   China

15

16   **Prof. Qingchu Li**

17   Email: liqingchu12@qq.com

18   Academy of Orthopedics, Orthopaedic Hospital of Guangdong Province

19   The Third Affiliated Hospital of Southern Medical University

20   China

21

22   # These authors contributed equally to this work.

23

24

Abstract

Additive Manufactured (AM) Polyether-ether-ketone (PEEK) orthopaedic implants offer new opportunities for bone substitutes. However, owing to its chemical inertness, the integration between PEEK implants and soft tissue represents a major challenge threatening the early success of the PEEK implants. Here we investigated the influence of hydroxyapatite (HA) fillers and porous structure of AM HA/PEEK scaffolds on the integration with soft tissue through *in-vitro* cellular experiments and *in-vivo* rabbit experiments. Among the animal experiments, HA/PEEK composite scaffolds with HA contents of 0, 20 wt%, 40 wt% and pore sizes of 0.8 mm, 1.6 mm were manufactured by fused filament fabrication. The results indicated that HA promoted the proliferation and adhesion of myofibroblasts on PEEK-based composites by releasing Ca^{2+} to active FAK and its downstream proteins, while the surface morphology of the scaffolds was also roughened by the HA particles, both of which led to the tighter adhesion between HA/PEEK scaffolds and soft tissue *in-vivo*. The macroscopic bonding force between soft tissue and scaffolds was dominated by the pore size of the scaffolds but was hardly affected by neither the HA content and nor the surface morphology. Scaffolds with larger pore size bonded more strongly to the soft tissue, and the maximum bonding force reached to 5.61 ± 2.55 N for 40 wt% HA/PEEK scaffolds with pore size of 1.6 mm, which was higher than that between natural bone and soft tissue of rabbits. Although the larger pore size and higher HA content of the PEEK-based scaffolds facilitated the bonding with the

1 soft tissue, the consequent outcome of reduced mechanical properties has to be

2 compromised in the design of the porous PEEK-based composite implants. The present

3 study provides engineering-accessible synergistic strategies on material components and

4 porous architecture of AM PEEK orthopaedic implants for improving the integration with

5 soft tissue.

6

7

8 **Keywords:** Polyether-ether-ketone composites; additive manufacturing; soft tissue;

9 porous scaffolds

10

11

1. Introduction

Polyether-ether-ketone (PEEK) has been considered as a candidate material in the next-generational orthopaedic implants[1] because of the advantages, including the excellent biocompatibility, similar density and mechanical properties to the natural bone as well as the radiolucency. Additive manufacturing (AM) of PEEK makes it possible to develop bone substitute with customized complex shapes[2], such as rib[3, 4], mandible[5], skull[6] and scapula[7], and has become an intense focus of research.

The success of PEEK orthopaedic implants depends on both osseointegration and integration with soft tissue, in which the former has been heavily investigated[8-12] while ignoring the latter in the field of orthopaedic implants. The integration with the soft tissue of the PEEK implants is essential for the reduction of dead space to prevent effusion, inflammation and infection, which threaten the early success of implants[13, 14]. Moreover, the integration of soft tissues such as muscles and tendons with the implant would reconstruct the original musculoskeletal mechanics, which is essential for restoring the mechanical function of the substituted bone. However, the poor integration of PEEK implants due to the biological inertness makes the clinical application in a dilemma[15, 16].

To promote the soft tissue integration or the osseointegration with implants, strategies such as composition, chemical modification, surface coating, biomolecular coating, surface morphology and porous design were attempted[17]. For example, some complicated nano-coating processes[11] or nutrient element decoration[12] method were used to improve the osseointegration of PEEK and obtain excellent outcome. However, the complexity of the processes made it difficult for these technologies to be applied in the engineering manufacturing, and to translate to clinics. Among the several strategies,

1 chemical modification and biomolecular coating may fail in moist-heat sterilization,

2 which is one of the most common approaches in medical device production. The risk of

3 peeling[18, 19] restricts the acceptance of surface coating in clinical practice. Therefore,

4 composition and porous structure were believed to be feasible from the perspective of

5 engineering implementation and clinical application.

6 Few filler materials such as HA[20], and beta-tricalcium phosphate (β-TCP)[21]

7 were employed to improve the integration with the soft tissue of PEEK implants. However,

8 it was hard to draw a generalized conclusion from current studies since the literature

9 reported contradictory results. The cytocompatibility of PEEK with 25% ceramic fillers

10 was compared with pure titanium (Ti) and zirconia by Guo et al. [22], and the results

11 illustrated similar cytocompatibility of soft tissue cells (mouse fibroblast cell line L929)

12 between the ceramic/PEEK composites and pure Ti. The cellular responses on PEEK, 5

13 wt% HA/PEEK and 5 wt% β-TCP/PEEK were similar according to Cruz et al. [21]. Both

14 studies did not support the view that bioactive ceramics in PEEK matrix is beneficial to

15 enhance the cell response of soft tissue, while Larsson et al. [23] demonstrated improved

16 soft tissue integration by HA coating on Ti abutments compared with that of the uncoated

17 surface. As seen in the existing knowledge, whether bioactive fillers positively affect the

18 soft tissue integration of PEEK-based composites remained in doubt.

19 The porous structure is vital for the mechanical integration between implants and

20 soft tissue because that only the mechanical interlock formed by the soft tissue ingrowth

21 in the porous structure can establish a stable mechanical connection between the soft

22 tissue and implants. Tikhilov et al. [24] contrasted the tensile strength of muscular tissue

23 attached with the porous Ti and that of solid plates, and the tensile strength of porous

24 plate was three times larger than that of solid plates. Su et al. [25] fabricated scaffolds

1 with two-levels porous architecture by sulfonation treatment of PEEK scaffolds made by

2 FFF, and the animal experiment suggested that the rougher surface created by sulfonation

3 treatment has no significant effect on mechanical bonding force between scaffolds and

4 soft tissue, despite the contribution on cell adhesion. It illustrated that the adhesion of

5 cells or tissues with the micro-structs did not significantly affect the mechanical bonding

6 between the porous implants and soft tissue. Nevertheless, the study of Feng et al. [26]

7 drew the different conclusions that the acid-etched rougher surface significantly enhanced

8 the bonding strength of the PEEK porous implants. The research from Lake et al. [27]

9 indicated that the bonding strength was higher in larger pore size within the range of 0.9

10 mm~4.9 mm from a porcine hernia repair model with polyethylene terephthalate (PET)

11 porous mesh. The implantation of porous Ti scaffolds in sheep paraspinal muscles from

12 Gordon et al. [28] pointed that pore size of 700 μm was most conducive to the in-growth

13 of soft tissue in a range of 200~1000 μm. It can be seen that less attention has been paid

14 to the mechanical bonding between PEEK porous implants and soft tissue, thus there was

15 no consensus on whether and how the porous structure affects the bonding of soft tissue

16 with PEEK implants.

17   In summary, the tight integration and further mechanical fixation between PEEK-

18 based implants and soft tissue were possibly the results of biological adhesion and

19 mechanical interlock. The addition of bioactive fillers, typically HA, in PEEK is a

20 promising approach with engineering feasibility to improve the adhesion with soft tissue,

21 which had been confirmed to be benefit for osseointegration, and the connective porous

22 structure is essential for the formation of interlock between soft tissue and implants.

23 However, it is difficult to obtain a coherent conclusion about the effect of fillers on the

24 adhesion of soft tissue, nor the consensus on the relationship between porous structure

and integration of soft tissue. Therefore, a systematic study of the effect of HA fillers and porous structure on the soft tissue integration of PEEK scaffolds would provide a theoretical basis for the development of AM PEEK-based composite orthopaedic implants that have good integration capabilities with both bone and soft tissue.

Herein, PEEK-based scaffolds with different HA contents and pore size were fabricated by fused filament fabrication (FFF). Cell response and rabbit experiments were conducted to investigate the effect of HA and pore size on the integration between soft tissue and PEEK-based scaffolds.

2. Materials and Methods

2.1 Material Preparation

HA/PEEK composite filaments with HA contents of 0, 20, and 40 wt% and a diameter of 1.75 mm were prepared by a V-type mixer (VH-12L, JiuDong, China) and twin-screw extruder (FLD 35, ACC Machine, China) from PEEK particles (150PF, Victrex, UK) and HA powder (HAP-08, Emperor, China) with an average particle size of 50 μm and 15 μm, respectively.

2.2 Fabrication of Scaffolds

A commercial FFF 3D printer (Surgeon 200, JUGAO-AM, China) was employed in this study. Cylinder scaffolds ($\Phi15\times5$ mm) with orthogonal porous architecture with different geometry were printed using HA/PEEK filaments with different HA contents. The geometry dimensions and HA contents involved in this study are presented in Table 1 and Figure 1-A. The FFF printing process parameters for the scaffolds with different pore sizes are presented in Table 2. The size of the micro-structs was determined by the nozzle diameter, while the pore size was determined by the distance between adjacent paths and layer thickness of the 3D printing process.

2.3 Characterization of Scaffolds

The surface morphology and section view of scaffolds were observed by scanning electron microscopy (SEM, S3000N, Hitachi, Japan). The structs size and pore size were also measured via SEM ($n=10$). The relative density φ_v was assessed by the ratio between the mass of scaffold and solid cylinder with same material components ($n=20$). Laser Scanning Confocal Microscope (LSCM, LEXT OLS4100, OLYMPUS, Japan) was used to observe the morphology of micro-structs and determine the roughness R_a ($n=5$). To evaluate the mechanical properties of the scaffolds, cubic specimens ($10\times10\times10$ mm) with the same material components and pore sizes were fabricated by the same process parameters. The relative elastic modulus and compression strength of the specimen were measured by a universal test machine (SANS CMT 4304, MTS, USA) with a loading speed of 3 mm/min ($n=3$). The deformation pattern of the scaffolds was captured by a high-speed video camera (i-SPEED 220, iX Cameras, UK).
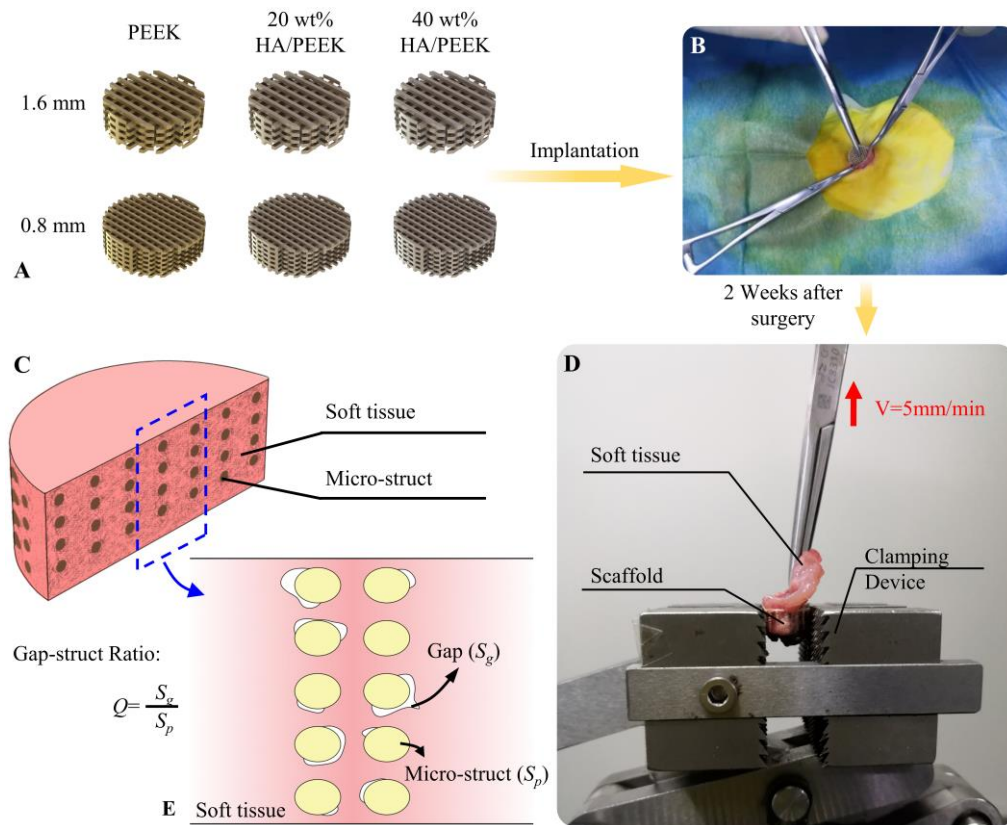
Figure 1. (A) 3D model of scaffolds with different pore sizes. (B) Implantation surgery. (C) Section of the retrieved scaffolds. (D) Quantization method of the Gap between micro-structs and soft tissue. (E) Measurement of separating force between soft tissue and scaffolds

Table 1. The HA contents and geometrical dimensions of different of scaffolds

No	HA Content /wt%	Pore Size /mm	Struct Size /mm	Theoretical Porosity /%
1	0	0.8	0.4	69.3
2	0	1.6	0.6	70.6
3	20	0.8	0.4	69.3
4	20	1.6	0.6	70.6
5	40	0.8	0.4	69.3
6	40	1.6	0.6	70.6

1   Table 2. 3D printing process parameters of scaffolds with different pore sizes

Process Parameters	Pore Size/mm	
	0.8	1.6
Nozzle Temperature/℃	420	420
Nozzle Diameter/mm	0.4	0.6
Layer Thickness/mm	0.2	0.2
Printing Speed/mm•s-1	30	30
Ambient Temperature/℃	20	20

2   2.4 Cell Experiments

3   Solid cylinder samples ($\Phi14 \times 2$ mm) were printed through the same process

4   parameters with different HA contents (0, 20 wt%, 40 wt%) as presented in Table 1. The

5   samples were ground and polished to minimize the effect of surface morphology on the

6   cell response. The water contact angles ($n=4$) were measured by previous study and no

7   significant difference was found among samples with different HA content[8]. Cylinder

8   samples with different HA contents ($n=4$ for each content for cytotoxicity, proliferation

9   and adhesion) were cleaned using normal saline solution for 5 mins and sterilized by

10   moist heat with temperature at 121℃ for 30 mins. All the samples were plated in a 24-

11   well plate for the cell experiment *in-vitro*. 1×10^5 myofibroblasts (MFBs) of rabbit were

12   seeded on the HA/PEEK samples.

13   *2.4.1 Releasing of Calcium ion*

14   The releasing of Calcium ion (Ca^{2+}) in HA/PEEK composites were carried out to

15   confirm that HA was successfully added to the PEEK matrix. Composites samples with

16   HA contents of 0, 20 wt% and 40 wt% ($n=6$) were soaked in 10 times the weight of

17   deionized water. Samples were soaked for 1, 3, 5, and 7 days at 37℃ and the Ca^{2+}

1   concentration was tested by ion chromatography. Deionized water was used as blank

2   control.

3   *2.4.2 Cytotoxicity*

4   The cytotoxicity was tested using CCK8 following the instructions from the

5   manufacturer's protocol (Sigma-Aldrich, USA) after culturing for 6 h. MFBs with the

6   same concentration were seeded on the 24-well plates as control. The cells were further

7   incubated at 37℃ for 2 h after the CCK8 reagent was added, and the OD value of the

8   culture medium at 450 nm was measured.

9   *2.4.3 Proliferation*

10   The proliferation experiment was tested using CCK8 following the instructions from

11   the manufacturer's protocol (Sigma-Aldrich, USA) after culturing for 24h and 72h. After

12   removing the culture medium, the cells were incubated at 37℃ for 2 h after the CCK8

13   reagent was added, and the OD value of the culture medium at 450 nm was measured.

14   *2.4.4 Adhesion*

15   MFBs with different samples were fixed in 4% paraformaldehyde for 30 mins after

16   culturing for 48 h, and stained with Alexa Fluor 594 phalloidin and 4', 6-diamidino-2-

17   phenylindole (DAPI). Cells morphology was observed by LSCM. The average area of

18   MFBs on confocal culture dishes was defined as 100%, and the degrees of extension of

19   the adherent cells on different samples were calculated.

20   *2.4.5 Western Blot*

21   MFBs with a density of 1×10^5 were inoculated on cylinder samples and were

22   collected after 7 days. The total protein of MFBs was extracted using

23   Radioimmunoprecipitation assay (RIPA) buffer, and the protein content of the cell lysates

24   was determined by bicinchoninic acid (BCA) assay. The protein expression of FAK, Talin,

Vinculin, Rho family GTase (RhoA, Rac1 and Cdc42) and F-actin were quantified by western blotting. Besides, the expression of these proteins in 20 wt% HA/PEEK and 40 wt% HA/PEEK groups treated with L-type calcium channel blocker verapamil (10μM) and FAK inhibitor PF573228 (5μM) was also analyzed.

2.4.6 Real-time Quantitative Polymerase Chain Reaction (RT-QPCR) analysis

MFBs were seeded on the cylinder samples for 7 days. After that, cells were collected and total RNA was extracted with TRIzol reagent (Invitrogen), followed by phenol chloroform-isopentyl ethanol extraction. Reverse transcription was performed with PrimeScript RT Reagent Kit (Takara) using 1000 ng of RNA in a 20 μL reaction system according to the manufacturer's instructions. RT-PCR was performed using SYBR Green PCR masterbatch (Takara) on the RT-PCR system (Applied Biosystems 7500). GAPDH is used as a housekeeping gene. All primer sequences used in this study are shown in Table 3. The expression of adhesion genes FAK, Talin, Vinculin, Rho family GTase (RhoA, Rac1 and Cdc42) and F-actin were analyzed in all samples, and the expression of these genes in 20 wt% HA/PEEK and 40 wt% HA/PEEK groups treated with L-type calcium channel blocker verapamil (10 μM) and FAK inhibitor PF573228 (5 μM).

Table 3. The corresponding primer sequences used for RT-QPCR

Gene	Forward primer (5'-3')	Reverse primer (5'-3')
GAPDH	TCGGAGTGAACGGATTTGGC	CCAGCATCACCCCACTTGAT
FAK	GGAGAAGTATGAGCTCGCCC	GTCTTGGTCCACTTGATCAGC
Talin	CAGATCAGCTCGGAGGGTTC	GATCGATGAGGTGCCCGATT
Vinculin	TCGAACAGCTCCGTCTAACAG	GCCAGGTTGTGGCATTCAAG
RhoA	GTCGCCCGAGCGATGG	ATTAACCGCGTGAGGGTTGT
Rac1	TGGGTAAGACTTGCCTGCTG	ACTTCAGGGTACCACTTCGC
Cdc42	TCTGAGTATGTGCCGACTGTTT	AAAGGGCTCTGGAGAGTGTT
F-actin	GTGCTTCTAGGCGGACTGTT	TCGGCCACATTGCAGAACTT

2.5 Animal Experiments

The scaffolds were subjected to ultrasonic cleaning for 5 mins using normal saline solution and autoclaved at 121℃ for 30 mins to sterilize before the surgery. The PEEK, 20 wt% HA/PEEK, and 40 wt% HA/PEEK scaffolds with pore sizes of 0.8 mm and 1.6 mm were randomly implanted into 24 New Zealand white rabbits weighing 2.5~3.0 Kg. The scaffolds were placed between chest muscles and muscular superficial fascia on both sides (Figure 1-B). Four scaffolds were implanted in each rabbit, and a totally 96 scaffolds were involved. Animals were euthanized after 3, 7 and 14 days of the implantation, and scaffolds were removed with soft tissue. The rabbits were purchased from Xi'an Jiaotong University Health Science Center. These experiments were conducted under the supervision and assessment of granted by Animal Ethics of Shaanxi Provincial Department of Science and Technology, China (SCXK (Shann) 2019-002), the ethical guidelines for animal studies were followed.

2.6 Histological characterization

The specimens were fixed by immersion in 4% paraformaldehyde for 48 h, embedded in paraffin and axially sectioned at 30 μm thickness using a hard-tissue slicer (BQ1600, LanMing Medical, China) as shown in Figure 1-C. Following HE staining, slices were observed with an Inverted fluorescence Microscope (IX53, OLYMPUS, Japan). To quantitatively analyze the ingrowth of soft tissue in the scaffolds, the histological images were imported into AutoCAD (Version 2014, Autodesk, USA), and the gaps' area between micro struct and tissue were measured with the outline of the different stained areas (Figure 1-D). Gap-Struct Ratio Q was defined as the gap area (S_g) to the area of cross-section of micro structs (S_p), thus Q quantified the adhesion of soft tissue to the scaffolds.

2.7 Mechanical Bonding Strength between Soft Tissue and Scaffolds

The separating forces between soft tissue and scaffolds were measured by a universal test machine (103A, Wance, China) with a 200 N load cell. As shown in Figure 1-E, a scaffold was fastened by a clamping device, and soft tissue was clamped by hemostatic forceps, which were fixed with the test frame of the machine. The separating test was carried out with a loading speed of 5 mm/min. The maximum force in the force-displacement curve was defined as the separating force between soft tissue and scaffolds (n=10).

2.8 Statistical Analysis

All data are expressed as the means ± standard deviation (SD). Statistical analysis was performed with one-way ANOVA by using SPSS software (Version 17.0, IBM, USA) and Tukey test. Statistically significant differences were defined as P<0.05 (*) and P<0.01 (**).

3. Results

3.1 Characterization of Scaffolds

The 3D surface morphology and the roughness values R_a of the micro-structs of various scaffolds obtained by the LSCM are presented in Figure 2-A and 2-I. The roughness increased with HA content, the surface of PEEK was the smoothest with R_a of 1.88 ± 0.76 μm and 0.76 ± 0.23 μm on scaffolds with the pore size of 0.8 mm and 1.6 mm, respectively. The roughest surface was on 40 wt% HA/PEEK scaffolds with R_a of 6.89 ± 1.29 μm and 6.54 ± 0.47 μm. The morphology of the surface and the section of scaffolds observed by the SEM are shown in Figure 2-B to 2-E. The micro-structs in PEEK scaffolds were smooth with minimal surface features, while the addition of HA roughened the surface. More particles were observed on the surface of the micro-structs

1   of 40 wt % HA/PEEK scaffolds than that of 20 wt%. Meanwhile, more and larger holes

2   were observed on the section view with the increase of HA content.

3   The measured structs size and pore size were presented in Figure 2-F and 2-G. The

4   micro-structs among scaffolds with different HA contents presented significant

5   differences. The measured pore size was 0.83 ± 0.06 mm and 1.58 ± 0.08 mm for scaffolds

6   with different designed pore sizes, respectively. As for the struct size, for scaffolds with

7   different geometrical dimensional was 0.36 ± 0.06 mm and 0.57 ± 0.05 mm. Although

8   the porosity of different groups of scaffolds was found to be significantly different

9   (Figures 2-H), all the average porosity values were in the range of 70~77%.

10   Figure 3 illustrates the equivalent elastic modulus, strength and deformation patterns

11   during compression of the cubic samples. The compressive elastic modulus and strength

12   were significantly associated with larger pore size, while the effect of HA content on both

13   elastic modulus and strength was not obvious. The PEEK scaffolds were gradually

14   compacted with the structs of the scaffolds being bent, while struct fracture were not

15   observed. But for the HA/PEEK scaffolds, struct fracture occurred during compression,

16   and this phenomenon became more apparent in 40 wt% HA/PEEK scaffolds.
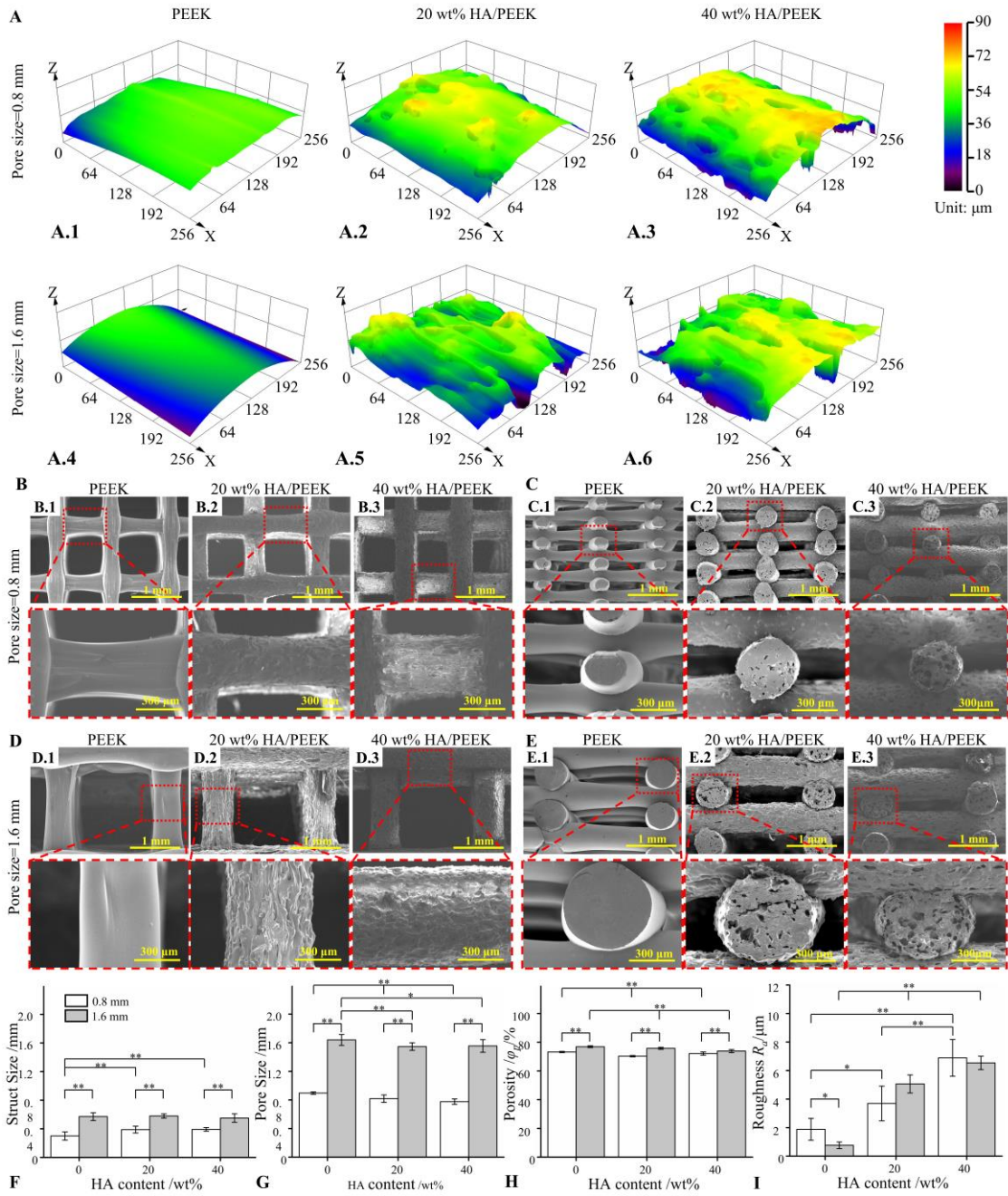
Figure 2. Characterization of the 3D printed PEEK Scaffolds. (A) LCSM images of micro-structs of different scaffolds. (B, C) SEM images of the surface of scaffolds with pore size of 0.8 and 1.6 mm. (D, E) SEM images of section view of the scaffolds with pore size of 0.8 and 1.6 mm. (F) Struct Size (n=10), (G) pore size (n=10), (H) porosity (n=20), (I) roughness of the scaffolds (n=5). (*: P <0.05; **: P <0.01)
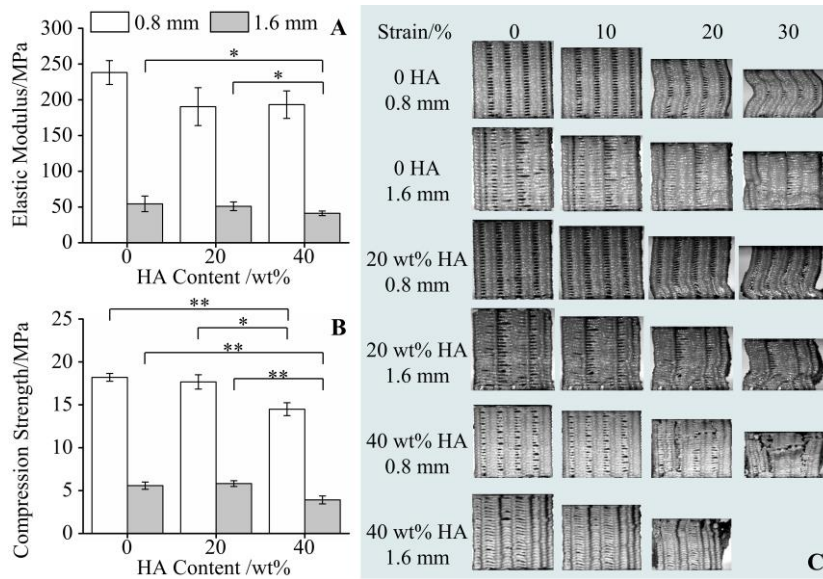
Figure 3. The mechanical test of the scaffolds. (A) The elastic modulus ($n=3$), (B) Compressive strength ($n=3$), (C) The deformation patterns of scaffolds with different HA contents and pore sizes.

3.2 Cell proliferation and spreading

The surface roughness R_a of samples with different contents was 0.123 ± 0.018 μm, 0.124 ± 0.032 μm and 0.131 ± 0.038 μm for the PEEK, 20 wt% HA/PEEK and 40 wt% HA/PEEK samples, respectively, and no significant differences between groups were observed. The results of Ca^{2+} releasing and cell response are presented in Figure 4. Figure 4-A showed that HA was added to PEEK matrix and higher content of HA/PEEK composites released more Ca^{2+}. As presented in Figure 4-B, insignificant difference among the OD value of control, PEEK and HA/PEEK groups, which illustrated that the PEEK and HA/PEEK materials were not toxic. Cell spreading and density (Figure 4-C) were both significantly raised with the increase of HA content. The adhesion morphology of the MFBs on different samples was shown in Figure 4-D. MFBs on the surface of HA/PEEK samples exhibited better extension than PEEK samples. The degree of cells

1 extension was further analyzed quantitatively and the results (Figure 4-E) indicated that

2 with the increase of HA content, the better of cell adhesion performance.

3
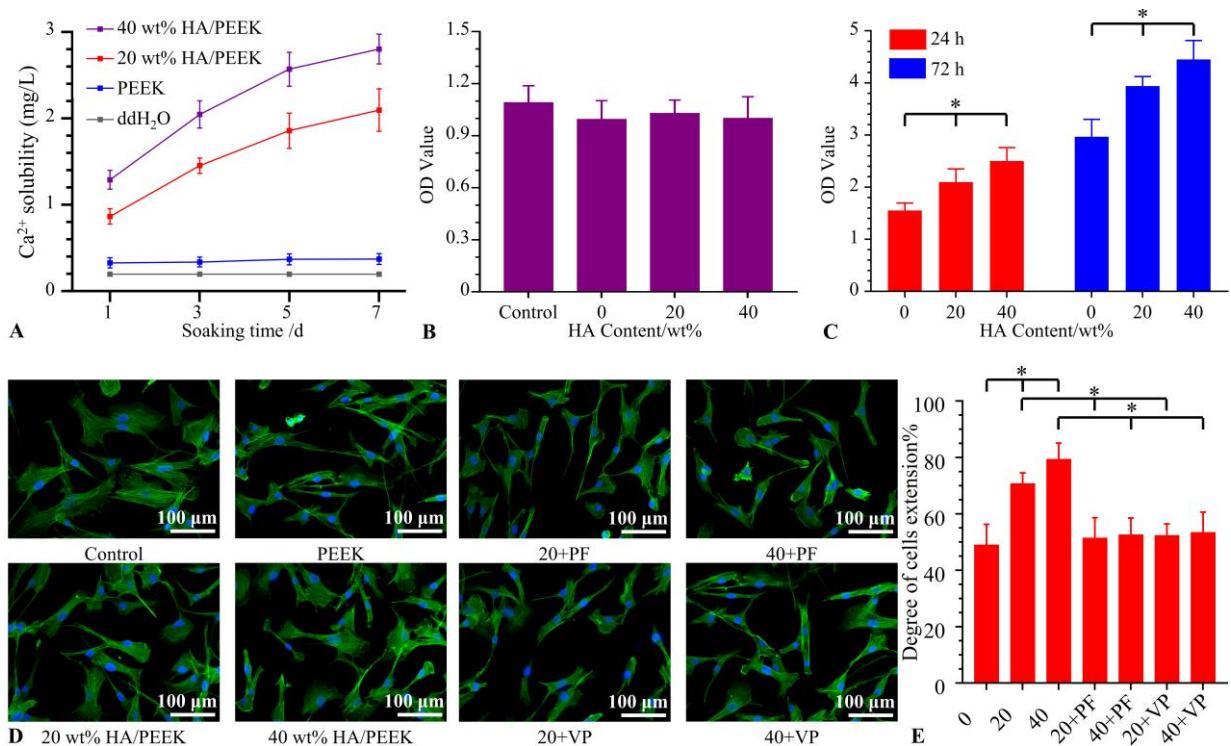
4   Figure 4. Results of Ca^{2+} releasing and cell response of samples with different HA

5   contents. (A) Ca^{2+} releasing (n=6). (B) cytotoxicity after culturing for 6 h (n=4). (C) cell

6   density on 24 h and 72 h (n=4). (D*) LSCM images of cells on samples after culturing

7   for 48 h. (E*) cell extension after culturing for 48 h (n=4). (*: P <0.05; **: P <0.01)

8   *Notes: (1) In 4-D and 4-E: 20+PF denotes 20 wt% HA/PEEK+ PF573228; 40+PF

9   denotes 40 wt% HA/PEEK+ PF573228; 20+VP denotes 20 wt% HA/PEEK+ verapamil;

10   40+VP denotes 40 wt% HA/PEEK+ verapamil; (2) In 4-E, 0 denotes pure PEEK, 20

11   denotes 20 wt% HA/PEEK; 40 denotes 40 wt% HA/PEEK

12   Western Blot was used to detect the expression of adhesive proteins (FAK, Talin,

13   Vinculin), Rho family GTases (RhoA, Rac1, and Cdc42) and F-actin cytoskeleton

14   proteins (Figure 5-A and 5-B). The expression levels of adhesive proteins (FAK, Talin,

19

1   Vinculin), Rho family GTase (RhoA, Rac1 and Cdc42) and F-actin cytoskeleton proteins

2   in 20 wt% and 40 wt% HA/PEEK groups were significantly higher than those in the

3   PEEK group. However, the expression levels of these proteins decreased significantly

4   after the addition of FAK inhibitor (PF573228) or verapamil, and there was no significant

5   difference with the PEEK group. These results indicated that HA in PEEK substrate could

6   promote the expression of adhesive proteins (FAK, Talin, Vinculin), Rho family GTase

7   (RhoA, Rac1 and Cdc42) and F-actin cytoskeleton protein, and FAK inhibitor (PF573228)

8   or verapamil can block the promotion triggered by HA. The expression of adhesion genes

9   (FAK, Talin, Vinculin), Rho family GTase (RhoA, Rac1, and Cdc42) and F-actin

10   cytoskeleton genes were detected by RT-QPCR (Figure 5-C and 5-D). The trends in the

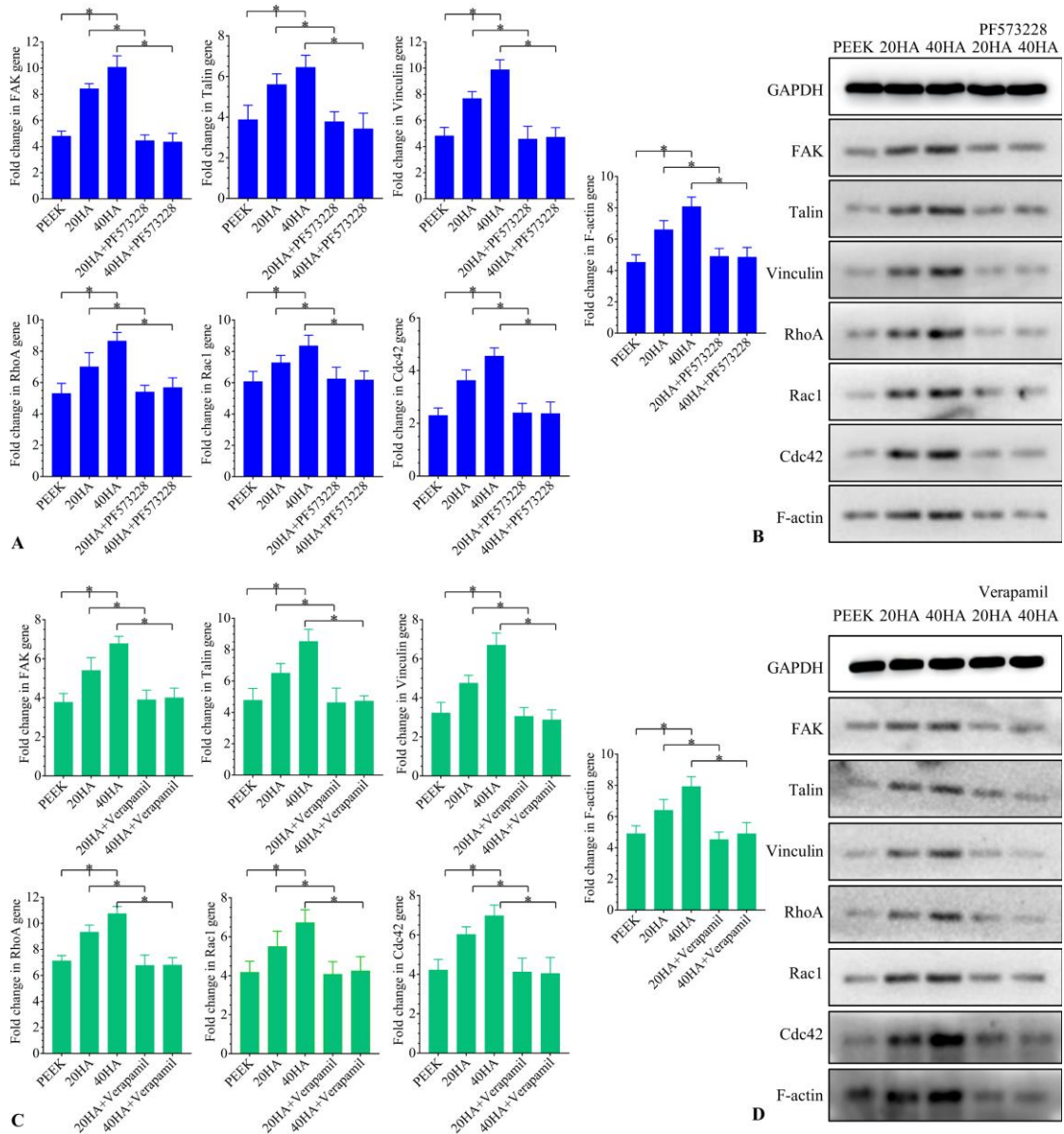11   expression levels of these genes were almost identical to those of the proteins.

Figure 5. Expression level of protein and gens involved in the adhesion of MFBs.

(A)(B) Western bolt analysis on total protein of FAK, Talin, Vinculin, RhoA, Rac1,

Cdc42 and F-actin cytoskeleton (7 days, *n*=4). (C)(D) Western bolt analysis on total

mRNA of FAK, Talin, Vinculin, RhoA, Rac1, Cdc42 and F-actin cytoskeleton (7 days,

n=4). Protein and gene expression levels was determined by normalizing to GAPDH.

(*: *P* <0.05; **: *P* <0.01)

3.3 Histological characteristics

The HE staining for the scaffolds 3 and 7 days after implantation are shown in Figure 6. More soft tissue was observed in the composite scaffolds with higher HA content, while similar trend was demonstrated at 7 days with difference being that the soft tissue has deeper color and clearer morphology, which was presumed to be the evidence of the new grown connective tissue.
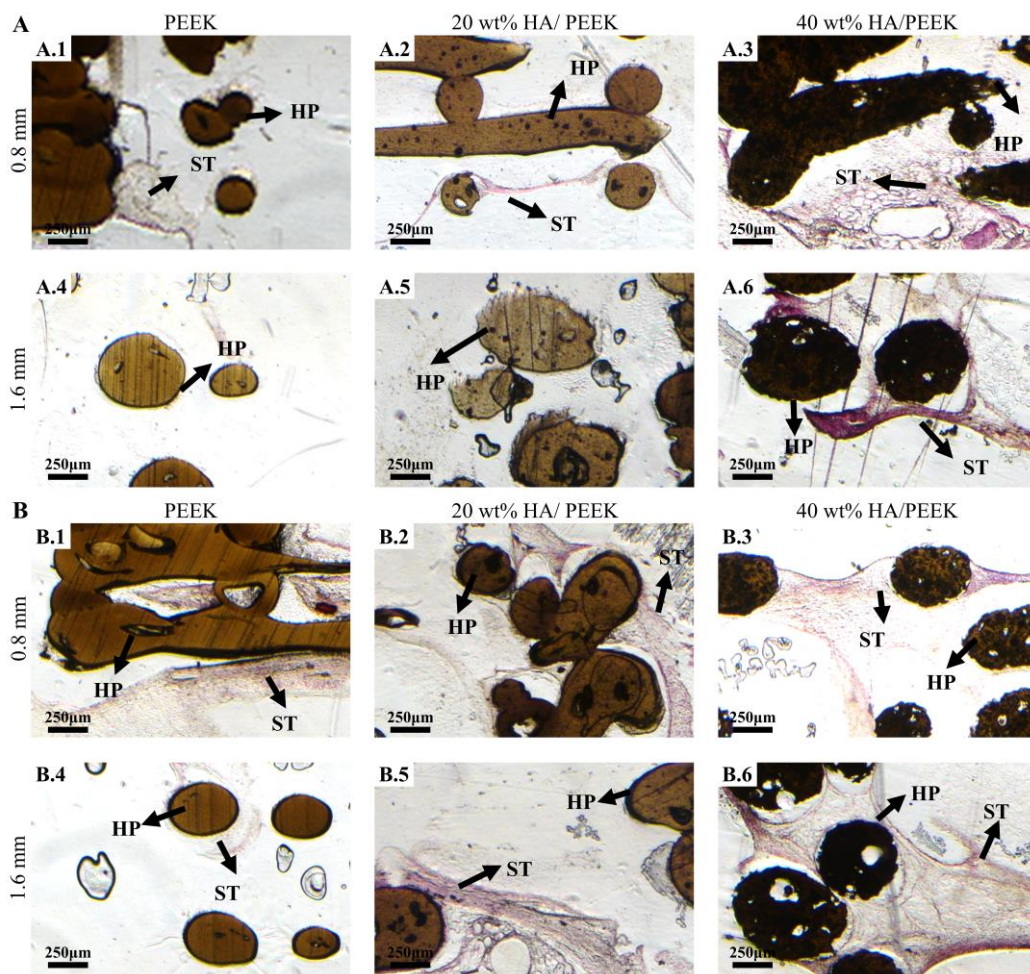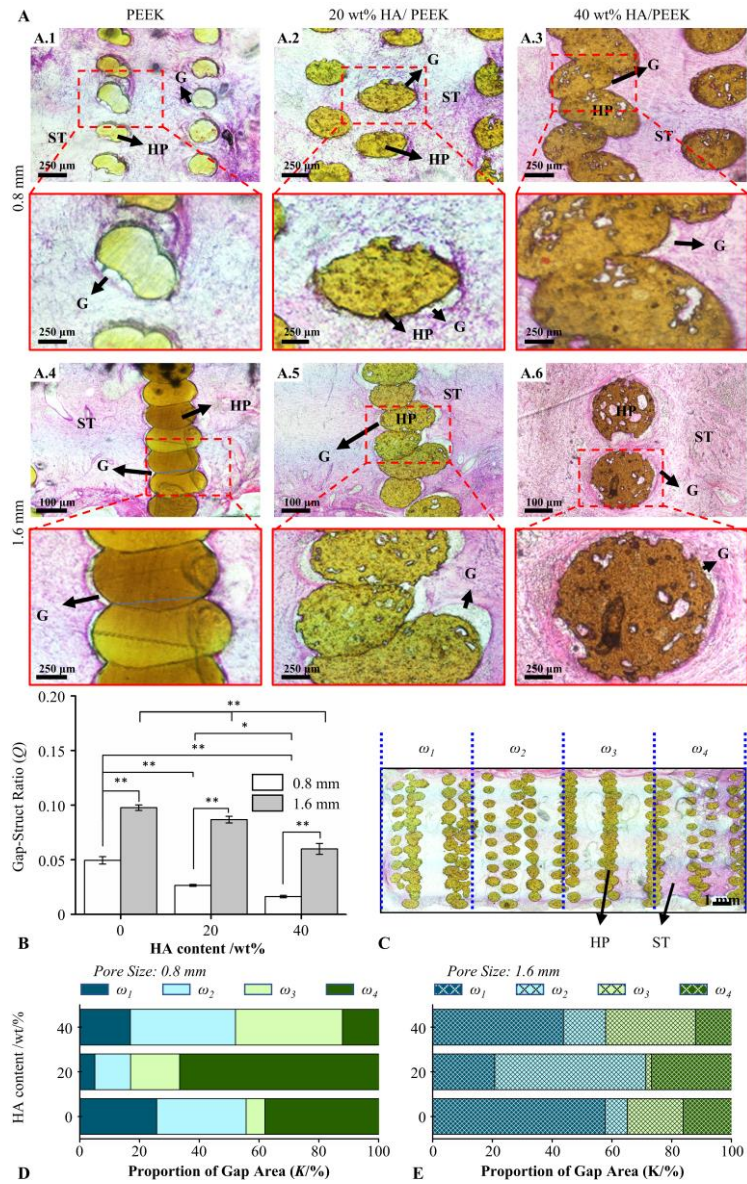

Figure 6. Histological characteristics of different scaffolds 3 and 7 days postoperatively.

(A) 3 days, (B) 7 days. (ST, Soft tissue; HP, micro structs of scaffolds)

1   Histological staining for the scaffolds retrieved at 14 days postoperatively are shown

2   in Figure 7. HE staining demonstrates that the new connective tissue almost filled the

3   pores in the scaffolds and no inflammation was observed. However, gaps between micro

4   structs of scaffolds and soft tissue were observed and the area of the gaps in the scaffolds

5   with the pore size of 0.8 mm appears smaller than that of 1.6 mm.

6   The gap between micro structs and soft tissue was quantified by the ratio Gap-Struct

7   Ratio Q and the results are presented in Figure 7-B. Obviously, the Q was reduced with

8   the increase of HA content, which illustrated that the gaps become smaller. When HA

9   contents were identical, the Q of scaffolds with the pore size of 0.8 mm was significantly

10   lower than that of 1.6 mm. Among all six groups, the maximum and minimum values of

11   Q were found in pure PEEK scaffolds with the pore size of 1.6 mm and 40 wt% HA/PEEK

12   scaffolds with the pore size of 0.8 mm, respectively. The whole section of a scaffold was

13   divided into four zones, as shown in Figure 7-C, where ω_1 and ω_4 located at the outside

14   of the cylinder scaffold while ω_2 and ω_3 located at the inside. The proportions of the gap

15   area in different zones in the total gap area of the whole section, which was defined as the

16   proportion of gap area (K/%), are illustrated in Figure 7-D and 7-E. It was indicated that

17   the maximum value of K was more likely to appear in Zone ω_1 or ω_4, namely near the

18   outside of the scaffolds, and this tendency was found in four (PEEK-0.8 mm, PEEK-1.6

19   mm, 20 wt% HA/PEEK-0.8 mm, 40 wt% HA/PEEK- 1.6 mm) out of all the six groups

20   of scaffolds.

21

Figure 7. Histological characteristics of different scaffolds 14 days postoperatively.
(A) HE staining of histological sections from different scaffolds. (ST, Soft tissue; G,
Gap between micro structs and soft tissue; HP, micro structs of scaffolds). (B) Gap-
Struct Ratio Q of different scaffolds (n=150~180 since each section contains these
numbers of sections of micro-structs, and 2 samples was sectioned for each group). (C)
Schematic drawing of the four zones in the HE stained sections. (D) The proportion of
gap area in different zones in the total gap area in the sections. (*: P <0.05; **: P <0.01)

24

3.4 Mechanical Bonding Strength between Soft Tissue and Scaffolds

The mechanical bonding between soft tissue and the scaffolds was evaluated by separating force. The representative force-displacement curves of PEEK scaffolds with the pore size of 0.8 mm and 1.6 mm are shown in Figure 8-A. The test loads increased with the displacement at the beginning of the curves, while the soft tissue was subjected to the tensile deformation (Figure 8-B). As the deformation increased, breakage of fibers occurred in the soft tissue (Figure 8-C), and the test load rose to the maximum. More fibers in the soft tissue were broken (Figure 8-D), and the test load was reduced with the displacement until the tissue encasing scaffolds was gradually separated from that in the scaffolds. Figure 8-E and 8-F present the scaffold before and after the test. Of concern is that few micro-structs of scaffolds were observed in the torn soft tissue (Figure 8-G), and it was frequently found in the HA/PEEK scaffolds. The separating force was defined as the maximum value of the load during the separating test, and the comparison of different groups was presented in Figure 8-H. At the same pore size, the separating forces among the scaffolds with various HA contents were not significantly different, whereas a significant difference was indicated between pore size of 0.8 mm and 1.6 mm in 20 wt% and 40 wt% HA/PEEK scaffolds. The maximum average separating force was 5.61 ± 2.55 N from 40 wt% HA/PEEK scaffolds with the pore size of 1.6 mm.
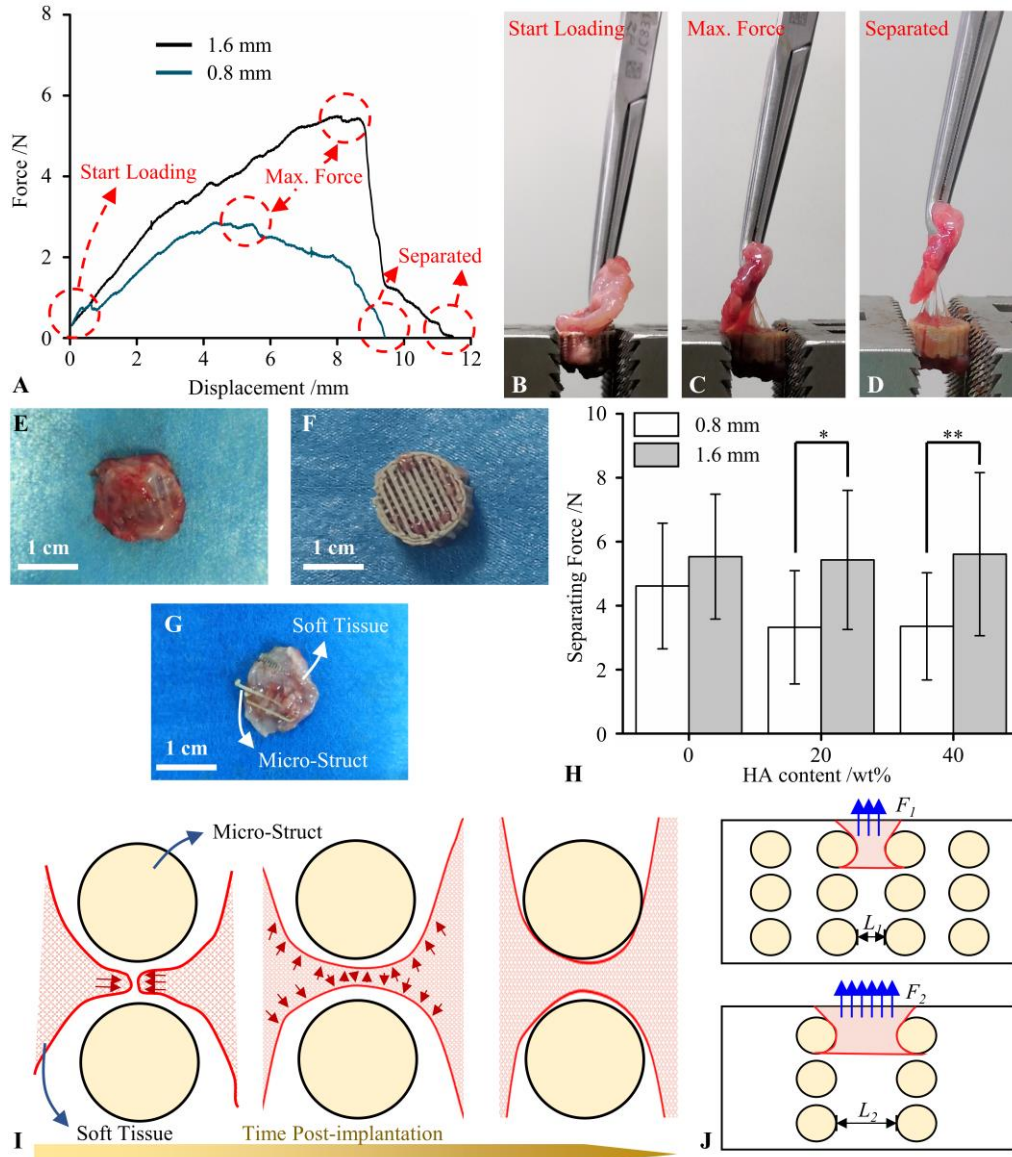
Figure 8. The separating force between soft tissue and scaffolds. (A) The typical force-displacement curves of PEEK scaffolds with pore sizes of 0.8 mm and 1.6 mm. (B)(C)(D) Representations of separating state at various stages. (E) The specimen before the separating test. (F) The scaffold which was separated from soft tissue. (G) The separated soft tissue which wrapped the micro-structs. (H) The separating forces of different scaffolds (n=12~15). (I) The in-growth pattern of the soft tissue in the scaffolds. (J) Schematic diagram of the separating forces of the scaffolds with different pore sizes.

4. Discussion

The poor integration with soft tissue caused by the chemical inertness represents a major challenge in AM PEEK orthopaedic implants. Rapid and tight adhesion and long-term fixation with soft tissue played an essential role in determining the success or failure of PEEK implants. With the consideration of engineering feasibility, PEEK-based composite material was believed to be a promising way to enhance the integration of implants with soft tissue. Few studies have addressed the influence of HA filters and the dimension of porous structure on the adhesion and mechanical bonding of PEEK implants with soft tissue. This study investigated the influence of HA fillers and pore size of AM HA/PEEK scaffolds on the integration with soft tissue through *in-vitro* cellular experiments and *in-vivo* rabbit experiments. Two indicators, the gap between micro-structs and soft tissue, as well as the bonding strength between the soft tissue and HA/PEEK scaffolds, were evaluated by quantitative investigation.

Scaffolds with different HA contents and pore sizes were fabricated by FFF in this study. The relative errors of measured pore size and struct size for scaffolds from all groups were lower than 10%, indicating scaffolds with reasonable accuracy. Among the scaffolds with the pore size of 0.8 mm, the struct size increased while the pore size decreased with HA content. The shrinkage of the HA/PEEK composites was believed to be the main factor driving this tendency. Since the struct size of the scaffold depends on the nozzle diameter of the 3D printer, it is currently not possible to adjust the struct size continuously, so the theoretical porosities of scaffolds with different pore sizes were not exactly equal. Nevertheless, the difference between the theoretical porosity was much less than that of porosity among each group of scaffolds whose maximum value was almost 7%, and it suggested the design and fabrication method used in this study to build

1   scaffolds was reasonable and accurate. Both SEM and LSCM observation demonstrated

2   that the surface of micro-structs became rough with the HA content, and more HA

3   particles were observed by SEM in the meantime. A previous study from Zheng et al. [29]

4   also pointed out that EDS spectral intensities of Calcium and Phosphorus increased with

5   the HA content in 3D printed HA/PEEK samples fabricated by the same machine.

6   FAK and its downstream proteins Talin and Vinculin are essential for the formation

7   of blotches that mediate cell adhesion. FAK not only affects the assembly and disassembly

8   of the blotches, but also the activity of Rho GTPases, which are involved in the dynamic

9   formation of the cytoskeleton. The cytoskeletal network of F-actin is regulated by rho-

10   GTPases, thereby affecting the change of cell morphology. Therefore, MFBs were seeded

11   on cylinder samples with different HA contents, and the expressions of key adhesion

12   proteins/genes FAK, Talin and Vinculin were analyzed by Western blot and RT-QPCR

13   respectively. It was found that the expressions of key adhesion proteins/genes increased

14   with the HA content in PEEK composites, and the expressions levels of these

15   proteins/genes were significantly decreased by FAK inhibitor PF573228 (5 μM). These

16   data indicate that increased HA content in PEEK composites could activate FAK, and

17   ultimately promote the formation of adhesion, and promote cell adhesion. Previous

18   studies have shown that intracellular Ca^{2+} accumulation activates adhesion kinase FAK.

19   The differences of Ca^{2+} release caused by different HA content resulted in different

20   intracellular Ca^{2+} concentration, which then affected the expression of the above adhesive

21   proteins/genes. MFBs was treated with verapamil (10 μM), an L-type calcium channel

22   blocker, to detect RhoA, Rac1, Cdc42 and F-actin protein and gene expression. The

23   results showed that the protein/gene expression of RhoA, Rac1, Cdc42 and F-actin could

24   be significantly increased with the increase of HA content and the concentration of the

1 intracellular Ca^{2+}, and blocked by the L-type calcium channel blocker verapamil (10 μM).

2 It indicated that the increase of HA content in PEEK scaffolds can activate Rho GTPases

3 through FAK by increasing intracellular Ca^{2+} concentration, and ultimately regulate the

4 cytoskeletal network of F-actin, thereby affecting cell morphology.

5   The toughness of the PEEK matrix was reduced by HA particles, thus the scaffolds

6 became easier to be brittle fractured. The mechanical properties of 3D printed HA/PEEK

7 solid samples investigated by Zheng et al.[29] and Vaezi et al.[30] confirmed that the

8 tensile strength was decreased by 48%, but the tensile elastic modulus was increased by

9 68% with HA contents of 30 wt%, comparing with pure PEEK, with the dramatically

10 reduced elongation at break. It led to the outcome that the structs of scaffolds were easier

11 to be bent and fractured during compression.

12   The soft tissue almost filled all the porous space within the scaffolds from the HE

13 staining 14 days postoperatively. However, gaps between soft tissue and micro-structs of

14 scaffolds were observed, which reflected that the growth pattern of soft tissue was not

15 adherent growth like the ingrowth of bone tissue. The ingrowth of soft tissue in the PEEK-

16 based scaffolds was speculated to follow the fill-adhere pattern as illustrated in Figure 8-

17 I, that is, the soft tissue would grow into the porous space at the beginning, then gradually

18 fill up the space as tissue grows, and finally attach and adhere to the surface of micro-

19 structs. Through the quantitative analysis of the HE stained sections at 14 days after

20 implantation, three main trends were obtained as follows: first, the geometry dimension

21 of the scaffolds had the most dramatic effect on the ingrowth of soft tissue; Second, the

22 HA content of the PEEK-based composite scaffolds also showed significant influence on

23 the adhesion of the soft tissue on scaffolds but not as drastic as the geometry dimension;

1 Third, the adhere of the soft tissue was tighter inside scaffolds compared with the external

2 part.

3 The gap-struct ratio (Q) of scaffolds with different geometry dimensions highlighted

4 a clear difference, which might attribute to the connectivity changed by the pore and struct

5 size. For the scaffolds with smaller pores and struct size, on the one hand, the individual

6 pores were closer and easier to connect, so that the connective distance of soft tissue in

7 adjacent pores became shorter. On the other hand, the smaller volume of individual pores

8 made it easier for soft tissue to fill up the pores. Therefore, the filling and attachment of

9 the soft tissue in the scaffolds with the pore size of 0.8 mm was better than that of 1.6

10 mm.

11 The gap between scaffolds and soft tissue was also narrowed by the increase of HA

12 contents. In the *in-vitro* experiment, the response of MFBs on cylinder samples with

13 different HA contents but similar roughness was observed. The results suggested that HA

14 contributes to the proliferation and extension of MFBs, which was believed to be one of

15 the main factors of the decreasing gap. Meanwhile, the rougher surface caused by the HA

16 particles might be conducive to reducing the gap. Narimatsu et al.[31] indicated that the

17 adhesion of rat fibroblast was promoted by the rougher surface of Ti samples. Feng et

18 al.[26] found that acid etching promoted the adhesion, spread and fibronectin secretion

19 of human skin fibroblasts (HSF) cells on the PEEK surface. Gheisarifar et al. [32] also

20 pointed out the benefit of a rougher surface on the adhesion of human gingival fibroblasts

21 (HGFs) on both Ti and PEEK. Taken together with the results presented in the cell

22 experiment of this study, the adhesion of MFBs cells was believed to be attributed to both

23 chemical composition and physical properties.

1   The difference of the gap-struct ratio internal and external the scaffolds was observed

2 from the sections of various scaffolds, but the association with the location was

3 independent of material content and geometry dimension. It might be caused by the

4 pulling from the surrounding musculature to the soft tissue within the scaffold *in-vivo*, or

5 from the retrieval operation.

6   From the perspective of mechanics, the integration between soft tissue and porous

7 scaffolds consists of two parts: the biological adhesion related to the biocompatibility and

8 bioactivity of material, as well as the mechanical interlock that corresponded with the

9 architecture and mechanical properties of the scaffolds. The results of the *in-vitro*

10 experiment go some way in revealing how the biological adhesion acts on the attachment

11 of soft tissue to the scaffold *in-vivo*. It was because the increased HA content improved

12 the Ca^{2+} content of the composites and rougher the surface, which led to the closer

13 attachment. The geometry dimension was demonstrated to be the most predominant factor

14 to affect the bonding between the soft tissue and scaffold. The average separating force

15 reached 5.53 ± 2.20 N for the scaffolds with the pore size of 1.6 mm, which was larger

16 than the separating force of 3.18 ± 1.05 N between the natural rib and muscular tissue

17 measured by Su et al.[25], suggesting that the requirement of stability between scaffolds

18 and soft tissue was satisfying. The reason why the porous structure with larger pores

19 possessed stronger bonding strength with soft tissue may be explained from two aspects

20 (Figure 8-J). In one aspect, the cross-sectional area of the soft tissue bundle divided by

21 the staggered micro-structs was larger in scaffolds with the pore size of 1.6 mm, so the

22 force it could endure was greater. In another aspect, the test process of separating force

23 could be regarded as the cutting of soft tissue by micro-structs in the scaffold, the stress

24 caused by the cutting was lower in the scaffolds with the pore size of 1.6 mm since the

1 struct size of the scaffolds was thicker than that of 0.8 mm. The stronger soft tissue and

2 the lower cutting stress by the scaffolds together resulted in the higher bonding strength

3 between soft tissue and scaffolds with larger pore size in this study. Although smaller gap

4 area was observed in the scaffolds with the pore size of 0.8 mm, indicating the better

5 biological adhesion, however, the benefit of the adhesion on the bonding strength between

6 tissue and scaffolds were limited on the top surface of the scaffolds but negligibly

7 contributed to the overall bonding strength. Lake et al. [27] investigated the impact of

8 pore size and shape of several polymer meshes on the mechanical strength of tissue

9 ingrowth in a porcine model of ventral hernia repair, the maximum peeling force was

10 increased by approximately 70% with larger pore size. The research of Feng et al. [26]

11 also corroborated the benefit of larger pore size, their results indicated that the pore size

12 of the specimens increased from 1.0 mm to 2.0 mm, the separation force was raised from

13 12.35 N to 31.56 N, a dramatic increase of 155%. Therefore, this paper argues that the

14 bonding strength between the soft tissue and porous implants relied mainly on the

15 mechanical interlock forming by the ingrowth of soft tissue in the porous structure.

16   Another finding that may deserve attention in the test of separating force was that

17 some micro-structs were found in the separated soft tissue. It demonstrated that the soft

18 tissue in the scaffolds was stronger than the limit in the tension of HA/PEEK porous

19 structure. The previous mechanical study indicated that the HA content decreased the

20 strength and toughness of the HA/PEEK samples[33], which led to the phenomenon that

21 some micro-structs were torn off during the separation test.

22   The ingrowth and bonding of soft tissue were investigated through both *in-vitro* and

23 *in-vivo* experiments, and geometry dimension was found to be the predominant factor that

24 affected the bonding between the soft tissue and scaffolds within the pore size and HA

1   content range in the present study. The influence of geometry dimension on the biological

2   adhesion and mechanical interlock was different: the adhesion of soft tissue was tighter

3   in the scaffolds with smaller pore and struct size, which illustrated better biological

4   adhesion, while the mechanical interlock became stronger with larger pore and struct size

5   since separating force was enhanced. The HA contents affected the adhesion of soft tissue

6   on the micro-structs of scaffolds through the combined effects of enhancement of

7   bioactivity of composite material and increase of surface roughness. Although the

8   investigation of the presented study indicated that the biological adhesion rarely

9   contributed to the bonding between porous structure and soft tissue, the tight adhesion is

10 of great significance for reducing postoperative pleural effusion and avoiding excessive

11 inflammatory responses[34]. Nevertheless, the addition of HA particles in the PEEK

12 matrix would decrease yield strength and toughness of the composite material, which is

13 harmful to the mechanical properties of the composite porous implants.

14   This paper may be instructive for the design and manufacturing of gradient porous

15 implants of PEEK-based composite material. Criteria such as bonding strength between

16 porous structure and soft tissue, avoiding inflammatory responses as well as mechanical

17 strength should be comprehensively considered in the design of porous implants with

18 composite material while different criteria place conflict demands on the material

19 components and geometry dimension of the porous structure. Therefore, the material

20 components and geometry dimension of implants that contact with soft tissue should be

21 rationally designed according to the clinical requirements, such as the management of

22 inflammation and the bonding with soft tissue, biomechanical environment and surgical

23 operation. The development of 3D printing provides a foundation for manufacturing

24 implants with both gradient material components and porous structure.

1 There were some limitations in the presented study. On the one hand, the scaffolds

2 were retrieved at a single time point after 14 days of the implantation, it consequent that

3 the space in the scaffolds was almost fulfilled by the soft tissue, which led to the lack of

4 investigation of the growth process of the soft tissue affected by both material components

5 and geometry dimension. On the other hand, only three different HA contents and two

6 pore sizes were set as independent variables in this study because of the limitation of

7 animal experiments, but in fact, it is hard to study the effect of a large number of

8 independent variables through animal experiments, thus numerical simulation could be

9 considered as an alternative way to investigate the effect of more factors on the bonding

10 of soft tissue.

11 **5. Conclusion**

12   The integration between soft tissue and HA/PEEK composite scaffolds was

13 investigated in this study. The effect of HA components and geometry dimensions on the

14 ingrowth and adhesion of soft tissue was studied through both *in-vitro* and *in-vivo*

15 experiment in which bonding strength between tissue and scaffolds were quantified. The

16 results indicated that the macroscopic bonding strength was dominated by the geometry

17 dimension, while the HA made a negligible contribution. However, HA has a facilitative

18 effect on the tight adhesion of the soft tissue to the PEEK-based composite scaffold,

19 which is vital for avoiding postoperative effusion. The present study provides

20 engineering-viable design principles on material components and geometry of AM PEEK

21 orthopaedic implants, and might help to settle the poor integration between PEEK and

22 soft tissue.

Acknowledgment

References

[1] Q. Li, Y. Zhang, D. Wang, H. Wang, G. He, Mater & Des, 116 (2017) 171-175.

[2] M. Rinaldi, T. Ghidini, F. Cecchini, A. Brandao, F. Nanni, Compos. Pt. B-Eng., 145 (2018) 162-172.

[3] J.F. Kang, L. Wang, C.C. Yang, L. Wang, C. Yi, J. He, D. Li, Biomech. Model. Mechanobiol., 17 (2018) 1083-1092.

[4] L. Wang, L. Huang, X. Li, D. Zhong, D. Li, T. Cao, S. Yang, X. Yan, J. Zhao, J. He, Y. Cao, L. Wang, Ann. Thorac. Surg., 107 (2019) 921-928.

[5] J. Kang, J. Zhang, J. Zheng, L. Wang, D. Li, S. Liu, J. Mech. Behav. Biomed. Mater., 116 (2021) 104335.

[6] A. De Barros, D. Brauge, R. Quehan, Z. Cavallier, F.E. Roux, E. Moyse, Turk. Neurosurg., 31 (2021) 142-147.

[7] D. Liu, J. Fu, H. Fan, D. Li, E. Dong, X. Xiao, L. Wang, Z. Guo, Journal of Bone Oncology, 12 (2018) 78-82.

[8] J. Zheng, H. Zhao, Z. Ouyang, X. Zhou, J. Kang, C. Yang, C. Sun, M. Xiong, M. Fu, D. Jin, L. Wang, D. Li, Q. Li, Composites Part B: Engineering, 232 (2022) 109508.

[9] M.M. He, Y. Huang, H. Xu, G.J. Feng, L.M. Liu, Y.B. Li, D. Sun, L. Zhang, Acta Biomater., 129 (2021) 18-32.

[10] S.D. Liu, Y.T. Zhu, H.N. Gao, P. Ge, K.L. Ren, J.W. Gao, Y.P. Cao, D. Han, J.H. Zhang, Mater. Sci. Eng. C-Mater. Biol. Appl., 88 (2018) 70-78.

[11] S. Wang, C.Y. Duan, W.Z. Yang, X.Y. Gao, J.C. Shi, J.P. Kang, Y. Deng, X.L. Shi, Z.G. Chen, Nanoscale, 12 (2020) 11936-11946.

[12] H. Wang, X. Fu, J. Shi, L. Li, J. Sun, X. Zhang, Q. Han, Y. Deng, X. Gan, Advanced Science, 8 (2021) 2101778.

[13] N.M. Bernthal, H.Y. Park, S.D. Zoller, F.A. Petrigliano, J. Am. Acad. Orthop. Surg., 27 (2019) E685-E690.

[14] M.B. da Cruz, J.F. Marques, G.M. Penarrieta-Juanito, M. Costa, J.C.M. Souza, R.S. Magini, G. Miranda, F.S. Silva, A. da Mata, J.M.M. Carames, Int. J. Oral Maxillofac. Implants, 34 (2019) 39-46.

[15] C.Z. Liao, Y.C. Li, S.C. Tjong, Polymers, 12 (2020) 48.

[16] E. Barker, L. AlQobaly, Z. Shaikh, K. Franklin, K. Moharamzadeh, Dentistry journal, 8 (2020).

[17] M.N. Abdallah, Z. Badran, O. Ciobanu, N. Hamdan, F. Tamimi, Adv. Healthc. Mater., 6 (2017) 24.

[18] M.Y. Zakaria, A. Sulong, N. Muhamad, M.R. Raza, M.I. Ramli, Mater. Sci. Eng. C-Mater. Biol. Appl., 97 (2019) 884-895.

[19] Q.Y. Chen, Y.L. Zou, W. Fu, X.B. Bai, G.C. Ji, H.L. Yao, H.T. Wang, F. Wang, Ceram. Int., 45 (2019) 4526-4534.

[20] B.I. Oladapo, S.A. Zahedi, S.O. Ismail, F.T. Omigbodun, O.K. Bowoto, M.A. Olawumi, M.A. Muhammad, Bio-Des. Manuf., 4 (2021) 44-59.

[21] M.B. da Cruz, J.F. Marques, G.M. Penarrieta-Juanito, M. Costa, J.C.M. Souza, R.S. Magini, G. Miranda, F.S. Silva, J.M.M. Carames, A. da Mata, J. Oral Implantol., 47 (2021) 9-17.

[22] L.N. Guo, R. Smeets, L. Kluwe, P. Hartjen, M. Barbeck, C. Cacaci, M. Gosau, A. Henningsen, Int. J. Mol. Sci., 20 (2019) 15.

[23] A. Larsson, M. Andersson, S. Wigren, A. Pivodic, M. Flynn, U. Nannmark, Clin. Implant Dent. Relat. Res., 17 (2015) E730-E735.

[24] R. Tikhilov, I. Shubnyakov, A. Denisov, V. Konev, I. Gofman, D. Starchik, P. Mikhailova, S. Bilyk, Hip Int.,   5.

[25] Y.W. Su, J.K. He, N. Jiang, H. Zhang, L. Wang, X. Liu, D.C. Li, Z.H. Yin, Mater & Des, 191 (2020) 8.

[26] X.K. Feng, H. Yu, H. Liu, X.N. Yu, Z.H. Feng, S.Z. Bai, Y.M. Zhao, Int. J. Mol. Sci., 20 (2019) 14.

[27] S.P. Lake, S. Ray, A.M. Zihni, D.M. Thompson, J. Gluckstein, C.R. Deeken, J. Mech. Behav. Biomed. Mater., 42 (2015) 186-197.

[28] M. Chimutengwende-Gordon, R. Dowling, C. Pendegrass, G. Blunn, PLoS One, 13 (2018) 17.

[29] J. Zheng, J. Kang, C. Sun, C. Yang, L. Wang, D. Li, J. Mech. Behav. Biomed. Mater., 118 (2021) 104475.

[30] M. Vaezi, C. Black, D.M.R. Gibbs, R.O.C. Oreffo, M. Brady, M. Moshrefi-Torbati, S.F. Yang, Molecules, 21 (2016) 21.

[31] I. Narimatsu, I. Atsuta, Y. Ayukawa, W. Oshiro, N. Yasunami, A. Furuhashi, K. Koyano, ACS Biomater. Sci. Eng., 5 (2019) 4976-4984.

[32] M. Gheisarifar, G.A. Thompson, C. Drago, F. Tabatabaei, M. Rasoulianboroujeni, J. Prosthet. Dent., 125 (2021) 155-164.

[33] J. Zheng, H. Zhao, E. Dong, J. Kang, C. Liu, C. Sun, D. Li, L. Wang, Mater. Sci. Eng. C, 128 (2021) 112333.

[34] A. Furuhashi, Y. Ayukawa, I. Atsuta, Y.D. Rakhmatia, K. Koyano, J. Clin. Med., 10 (2021) 9.